

DTIC FILE COPY

②

GL-TR-90-0060

AD-A224 391

Satellite Measurements of Magnetospheric Poynting Flux

**J. F. Vickrey
M. C. Kelley
D. J. Knudsen**

**DTIC
ELECTE
JUL 30 1990
S D**

**SRI International
333 Ravenswood Avenue
Menlo Park, CA 94025**

9 March 1990

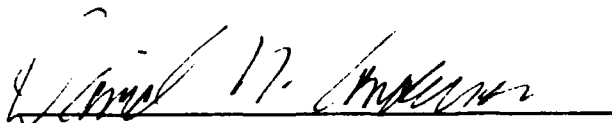
**Final Report
August 1968-March 1990**

Approved for public release; distribution unlimited

**GEOPHYSICS LABORATORY
AIR FORCE SYSTEMS COMMAND
UNITED STATES AIR FORCE
HANSCOM AIR FORCE BASE, MASSACHUSETTS 01731-5000**

80 07 30 198

"This technical report has been reviewed and is approved for publication




Contract Manager



DAVID N. ANDERSON
Branch Chief

FOR THE COMMANDER


ROBERT A. SKRIVANEK
Division Director

This report has been reviewed by the ESD Public Affairs Office (PA) and is releasable to the National Technical Information Service (NTIS).

Qualified requestors may obtain additional copies from the Defense Technical Information Center. All others should apply to the National Technical Information Service.

If your address has changed, or if you wish to be removed from the mailing list, or if the addressee is no longer employed by your organization please notify GL/IMA, Hanscom AFB, MA 01731. This will assist us in maintaining a current mailing list.

Do not return copies of this report unless contractual obligations or notices on a specific document requires that it be returned.

UNCLASSIFIED

SECURITY CLASSIFICATION OF THIS PAGE

REPORT DOCUMENTATION PAGE				
1a REPORT SECURITY CLASSIFICATION Unclassified		1b RESTRICTIVE MARKINGS		
2a SECURITY CLASSIFICATION AUTHORITY		3 DISTRIBUTION AVAILABILITY OF REPORT		
2b DECLASSIFICATION/DOWNGRADING SCHEDULE		Approved for public release; distribution unlimited		
4 PERFORMING ORGANIZATION REPORT NUMBER(S) SRI Project 2592		5 MONITORING ORGANIZATION REPORT NUMBER(S) GL-TR-90-0060		
6a NAME OF PERFORMING ORGANIZATION SRI International	6b OFFICE SYMBOL (if applicable)	7a NAME OF MONITORING ORGANIZATION Geophysics Laboratory		
6c ADDRESS (City, State, and ZIP Code) 333 Ravenswood Avenue Menlo Park, California 94025		7b ADDRESS (City, State, and ZIP Code) Hanscom Air Force Base Bedford, Massachusetts 01731-5000		
8a NAME OF FUNDING SPONSORING ORGANIZATION	8b OFFICE SYMBOL (if applicable)	9 PROCUREMENT INSTRUMENT IDENTIFICATION NUMBER F19628-86-K-0044		
8c ADDRESS (City, State, and ZIP Code)		10 SOURCE OF FUNDING NUMBERS		
		PROGRAM ELEMENT NO. 61102F	PROJECT NO. 2310	TASK NO. G9 WORK UNIT ACCESSION NO. AB
11 TITLE (Include Security Classification) Satellite Measurements of Magnetospheric Poynting Flux				
12 PERSONAL AUTHOR(S) J. F. Vickrey, M. C. Kelley, D. J. Knudsen				
13a TYPE OF REPORT Final Technical	13b TIME COVERED FROM 08/86 TO 03/90	14 DATE OF REPORT (Year Month, Day) 1990 March 9	15 PAGE COUNT 36	
16 SUPPLEMENTARY NOTATION				
17 COSATI CODES			18 SUBJECT TERMS (Continue on reverse if necessary and identify by block number)	
FIELD	GROUP	SUB-GROUP	Magnetospheric Poynting Flux	
			Electric and Magnetic Field Fluctuations	
			Joule heating	
19 ABSTRACT (Continue on reverse if necessary and identify by block number)				
<p>The first satellite observations of the Magnetospheric Poynting flux are presented for two passes of the HILAT satellite over the northern polar regions. The simultaneously measured energy input due to precipitating particles is also presented. The Poynting flux is in general agreement with an independent estimate of the Joule dissipation in the upper atmosphere. However, there are localized regions in both orbits of net upward Poynting flux, suggesting a neutral wind dynamo. Evidence for the existence of propagating Alfvén waves as well as steady state current systems closed in the ionosphere are also presented.</p>				
20 DISTRIBUTION/AVAILABILITY OF ABSTRACT <input type="checkbox"/> UNCLASSIFIED/UNLIMITED <input type="checkbox"/> SAME AS RPT. <input type="checkbox"/> DTIC USERS			21 ABSTRACT SECURITY CLASSIFICATION Unclassified	
22a NAME OF RESPONSIBLE INDIVIDUAL David Anderson			22b TELEPHONE (Include Area Code)	22c OFFICE SYMBOL GL/LIM

DD FORM 1473, 84 MAR

83 APR edition may be used until exhausted
All other editions are obsolete

SECURITY CLASSIFICATION OF THIS PAGE

UNCLASSIFIED

TABLE OF CONTENTS

SUMMARY	v
I. INTRODUCTION	1
II. QUASI DC POYNTING FLUX MEASUREMENTS	
MADE BY THE HILAT SATELLITE	3
III. HILAT MEASUREMENTS OF QUASI DC POYNTING FLUX	7
IV. AC POYNTING FLUX CONSIDERATIONS	16
V. CONTINUED APPLICATIONS	20
REFERENCES	21
APPENDIX A: Derivation of the Poynting Flux for a Simple Situation . .	A-1
APPENDIX B: Derivation of the Expected Characteristics of Electric-	
and Magnetic-Field Fluctuation Signatures for Steady State	
Currents and Alfvén Waves	B-1



Accession For	
NTIS CRA&I	<input checked="" type="checkbox"/>
DTIC TAB	<input type="checkbox"/>
Unannounced	<input type="checkbox"/>
Justification	
By	
Distribution /	
Availability Codes	
Dist	Avail and for Special
A-1	

LIST OF ILLUSTRATIONS

1. **S1:** Surface through which magnetospheric Poynting flux \vec{P} enters the upper atmosphere. **S2:** The earth's surface, being a good conductor requires $E_{\perp} \equiv 0$ and hence $\vec{P} \equiv 0$. **S3:** Assuming that magnetic field lines are straight and vertical as well as the fair weather electric field implies that $\vec{P} \cdot \vec{S}_3 \equiv 0$ 4
2. Magnetic field fluctuations measured by the HILAT satellite on days 164, and 122, 1984. 8
3. Poynting flux, field-aligned current, and precipitating electron energy flux measured on day 164. The panels on the right show the spacecraft trajectory in geographic (upper) and geomagnetic (lower) coordinates. The loci of the E- and F-region penetration of the ray path to the satellite are also indicated. 10
4. Comparison of the estimated Joule heating rate and Poynting flux measured by HILAT on day 164, 1984. 12
5. Poynting flux, field-aligned current, and precipitating electron energy flux measured on day 122, 1984. 13
6. Sum of Poynting flux and total precipitating electron energy flux measured on day 122, 1984. 15
7. Power spectral density of Poynting flux and measured impedance for a steady state, ionospherically closed current system. 17
8. Power spectral density of Poynting flux and measured impedance for what appears to be an Alfvén wave. 18

SUMMARY

We have examined in detail the electromagnetic energy input into the upper atmosphere in the form of Poynting flux. It is shown that a spacecraft that is instrumented to simultaneously measure both the electric and magnetic fields, and that is at an altitude high enough to ignore collisions but below any field-aligned potential drops, can routinely measure the total electromagnetic energy flux into the atmosphere along its trajectory. Examples from the HILAT satellite are presented. These illustrate the feasibility of the technique and even suggest some small regions of upward Poynting flux driven by low altitude neutral winds.

Conversion factors for U.S. Customary to metric (SI) units of measurement

MULTIPLY \longrightarrow	BY \longrightarrow	TO GET
TO GET \longleftarrow	BY \longleftarrow	DIVIDE
angstrom	1.000 000 X E -10	meters (m)
atmosphere (normal)	1.013 25 X E +2	kilo pascal (kPa)
bar	1.000 000 X E +2	kilo pascal (kPa)
barn	1.000 000 X E -28	meter ² (m ²)
British thermal unit (thermochemical)	1.054 350 X E +3	joule (J)
calorie (thermochemical)	4.184 000	joule (J)
cal (thermochemical)/cm ²	4.184 000 X E -2	mega joule/m ² (MJ/m ²)
curie	3.700 000 X E +1	*giga becquerel (GBq)
degree (angle)	1.745 329 X E -2	radian (rad)
degree Fahrenheit	$t_F = (t_C + 459.67)/1.8$	degree kelvin (K)
electron volt	1.602 19 X E -19	joule (J)
erg	1.000 000 X E -7	joule (J)
erg/second	1.000 000 X E -7	watt (W)
foot	3.048 000 X E -1	meter (m)
foot-pound-force	1.355 818	joule (J)
gallon (U.S. liquid)	3.785 412 X E -3	meter ³ (m ³)
inch	2.540 000 X E -2	meter (m)
jerk	1.000 000 X E +9	joule (J)
joule/kilogram (J/kg) (radiation dose absorbed)	1.000 000	Gray (Gy)
kilotons	4.183	terajoules
kip (1000 lbf)	4.448 222 X E +3	newton (N)
kip/inch ² (ksi)	6 894 757 X E +2	kilo pascal (kPa)
ktap	1.000 000 X E +2	newton-second/m ² (N-s/m ²)
micron	1.000 000 X E -6	meter (m)
mil	2.540 000 X E -5	meter (m)
mile (international)	1.609 344 X E +3	meter (m)
ounce	2.834 952 X E -2	kilogram (kg)
pound-force (lbs avoirdupois)	4.448 222	newton (N)
pound-force inch	1.129 848 X E -1	newton-meter (N m)
pound-force/inch	1 751 268 X E +2	newton/meter (N/m)
pound-force/foot ²	4.788 026 X E -2	kilo pascal (kPa)
pound-force/inch ² (psi)	6 894 757	kilo Pascal (kPa)
pound-mass (lbm avoirdupois)	4.535 924 X E -1	kilogram (kg)
pound-mass-foot ² (moment of inertia)	4.214 011 X E -2	kilogram-meter ² (kg m ²)
pound-mass/foot ³	1.601 846 X E +1	kilogram/meter ³ (kg/m ³)
rad (radiation dose absorbed)	1.000 000 X E -2	**Gray (Gy)
roentgen	2.579 760 X E -4	coulomb/kilogram (C/kg)
shake	1.000 000 X E -8	second (s)
slug	1 459 390 X E +1	kilogram (kg)
torr (mm Hg, 0° C)	1.333 22 X E -1	kilo Pascal (kPa)

*The becquerel (Bq) is the SI unit of radioactivity; 1 Bq = 1 event/s.

**The Gray (Gy) is the SI unit of absorbed radiation.

A more complete listing of conversions may be found in "Metric Practice Guide E 380-74," American Society for Testing and Materials.

I. INTRODUCTION

Energy input to the earth's atmosphere due to the interaction between the solar wind and the magnetosphere occurs primarily at high latitudes. Kinetic energy is deposited through the precipitation of energetic particles and electromagnetic energy is dissipated via Joule heating. Either energy source can dominate the other at a given location and local time. In fact, *Vickrey et al.* (1982) showed that, although the daily averages of the energy flux from particles and Joule heating are comparable in the auroral oval, there is a tendency for the two to be anticorrelated. Based on Chatanika incoherent scatter radar measurements, those authors found the morning sector (westward electrojet) particle energy deposition rate to be generally larger than that in the premidnight sector eastward electrojet. The Joule heating rate has the opposite asymmetry about midnight. This tendency for anticorrelation is easily understood. Where the particle flux is relatively hard, ionization is produced at lower altitudes. Because the Hall mobility peaks at a lower altitude than the Pedersen mobility, the currents associated with hard particles have a greater tendency to flow in the Hall, rather than the Pedersen direction. Because Hall currents flow in a direction that is orthogonal to the electric field, they are by definition non-dissipative. On a global scale, however, Joule heating is thought to be larger than particle energy deposition because it is spread over a wider range of latitudes.

Remote sensing of particle precipitation is straightforward and is regularly performed by polar orbiting spacecraft. Joule heating, on the other hand, is not yet routinely monitored and its estimation usually requires severe approximations such as neglect (or very simplistic modelling) of the atmospheric wind; e.g. *Vickrey et al.* (1982). In this report we show that the electromagnetic energy flux into the atmosphere can be reliably measured by polar orbiting spacecraft at altitudes in the range 400–1000 km by determination of the vertical component of the Poynting

flux. Since this measurement is of a local quantity, no assumptions are required concerning the relative orientation of the spacecraft velocity and current sheets such as are needed in determination of Birkeland currents. Moreover, neutral winds, the ionospheric conductivity, and conductivity gradients are all accounted for in the measurement.

A theoretical discussion for the elementary case of energy dissipation in a resistive wire is presented in Appendix A. In the following sections, analyses of the Poynting flux measured during two passes of the HILAT satellite are presented. These events are of interest in their own right and show some of the usefulness of the concept. Continued, long term studies of the effect of solar activity on the atmosphere can benefit greatly from this measurement technique. It is hoped that more refined algorithms can eventually be applied to ISTP and DMSP measurements to estimate the total energy input into the upper atmosphere.

II. QUASI DC POYNTING FLUX MEASUREMENTS MADE BY THE HILAT SATELLITE

A derivation of the Poynting flux for a simple wire is presented in Appendix A. For our application to the problem of magnetosphere-ionosphere coupling, we first consider the volume enclosed by the surface of the earth and a "cap" covering all latitudes above say 50° . The cap is located at an altitude which is not crucial but which is between ~ 400 and 1000 km. (In what follows, we assume that it is the satellite's orbital altitude.) This height is chosen to be high enough that particle collisions are rare but below any region of significant field-aligned electric fields associated with the aurora. We assume that the zonal component of the perpendicular electric field goes smoothly to zero at the low latitude edge of S1, that the magnetic field lines are everywhere vertical, and we ignore curvature of the magnetic field lines over this height range. The volume of interest, shown in Figure 1, is then bounded by the high altitude cap, S1, the surface of the earth, S2, and the surface S3 linking the cap and the earth. Since the earth is a good conductor the electric field vanishes on S2 and the Poynting flux is zero across it. If no thunderstorms are located near the boundary then we can assume that the fair weather electric field is vertical and the Poynting flux across S2 is also zero. This implies that the entire electromagnetic power dissipated in the volume may be found by integrating the Poynting flux across S1. Since S1 is perpendicular to B_0 , the power input to the earth's atmosphere in the high latitude zone is given by

$$W_T = \frac{1}{\mu_0} \int_{S_1} \int (\underline{E}_o \times \delta B_\perp) \cdot d\hat{s} \quad (1)$$

where \underline{E}_o is the perpendicular electric field on S1 and δB_\perp is the deviation of the total magnetic field from the undisturbed value in the plane perpendicular to B_0 .

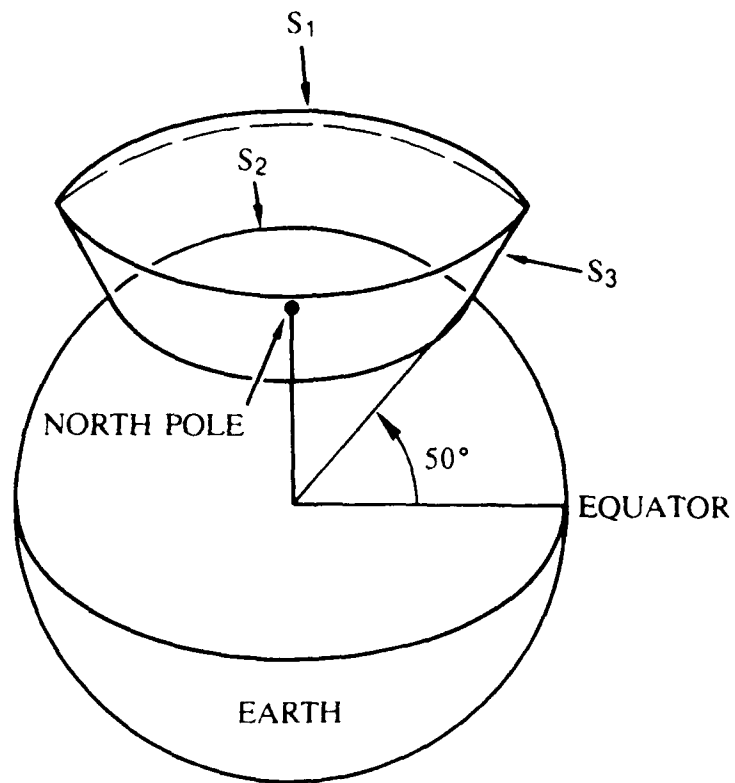


Figure 1. **S1:** Surface through which magnetospheric Poynting flux \vec{P} enters the upper atmosphere. **S2:** The earth's surface, being a good conductor requires $E_\perp \equiv 0$ and hence $\vec{P} \equiv 0$. **S3:** Assuming that magnetic field lines are straight and vertical as well as the fair weather electric field implies that $\vec{P} \cdot \vec{S}_3 \equiv 0$.

As we shall see, this energy is quite substantial, often locally larger than the input of energy via precipitating particles. Furthermore, existing spacecraft instrumentation is quite capable of determining this quantity in an unambiguous manner, albeit only along one trajectory, by measuring the vector electric and magnetic fields. A local measurement of $E_0 \times \delta B_\perp$ at typical ionospheric satellite altitudes yields the local power input to the earth's atmosphere. It is important to note that no geometric assumptions are necessary to find this quantity, unlike those required to determine, for example, J_\parallel from magnetic field measurements along a trajectory (which can only yield one component of $\nabla \times B$). It is also true that the Poynting flux yields the correct energy input even if a neutral wind is present in the ionosphere, which is almost always the case. In fact if, as has been suggested, a "flywheel" effect occurs such that accelerated neutral winds maintain the circulation of plasma during decaying magnetic activity, then the Poynting flux will be upward. A detection of upward Poynting flux would then be unambiguous evidence for such a flywheel effect.

We can also compare the present results to recent publications of correlations between the component of the electric field along a satellite trajectory with the component of the magnetic field detected across the trajectory. These correlations are sometimes excellent (e.g., *Sugiura et al.*, 1982) and sometimes not so good (*Burke et al.*, 1982). These authors point out that assuming that the current sheets are perpendicular to the trajectory and that the ionospheric conductivity is uniform, the charge neutrality condition $\nabla \cdot J \equiv 0$ implies that

$$\frac{E_z}{\delta B_y} = \frac{1}{\mu_0 \Sigma_p} \quad (2)$$

where Σ_p is the height-integrated Pedersen conductivity. Well-correlated data then imply uniform Σ_p as well as provide a measure of that quantity. However, gradients in Σ_p , neutral winds, and non-L-shell aligned current sheets all make the ratio above invalid and have been used to explain the cases when the correlation is not good. Moreover, the above relation (2) assumes that static currents closing through the ionosphere are being sampled. If, however, the electrodynamic perturbations

were due to a propagating Alfvén wave, the ratio of $\mu_0 E_z / \delta B_y$ would yield the intrinsic impedance of the medium, not the inverse of the height integrated Pedersen conductivity. This is discussed in detail in Section IV. The Poynting flux, on the other hand, does not suffer from these ambiguities, and, furthermore, seems a more fundamental quantity.

Before discussing the HILAT satellite measurements, one additional comment is of interest. As noted above, the magnetospheric electric field maps deep into the stratosphere. If we acknowledge that there is very little dissipation of magnetospherically imposed electrical energy in the troposphere, then it follows that the perturbation magnetic field due to auroral currents near the surface of the earth (δB) must be parallel to the mapped electric field (E). In turn, this is equivalent to the oft-quoted statement that ground magnetometers respond only to overhead Hall currents. The Poynting flux argument can thus be used to make this point without the necessity to show that the magnetic fields from Birkeland currents cancel those from Pedersen currents. Balloon data taken in the stratosphere have been compared to nearby ground magnetic field data and E has been found to be parallel to δB (*Mozer and Serlin, 1969*).

III. HILAT MEASUREMENTS OF QUASI DC POYNTING FLUX

In this section we present two examples of Poynting flux measurements in the high latitude ionosphere. The instruments used were not optimized for measurement of this parameter. Yet the results are quite reasonable and support the theoretical discussion given above. We believe the Poynting flux measurement concept is worthy of pursuit with more sensitive instruments and more stable measurement platforms.

The data come from the HILAT satellite which measures the vector magnetic field using a fluxgate magnetometer and deduces the electric field from an ion drift meter. Each of the three components of the magnetometer was sampled at a 20 Hz rate. The cross-track drift of the plasma is sampled at a 4 Hz rate. Unfortunately the in-track drift component is only available once per second since it requires a sweep of the retarding potential analyzer. These drift data yield the electric field component perpendicular to B_0 which is also necessary for a full Poynting flux determination.

The spacecraft is gravity gradient stabilized but suffers attitude perturbations from thermal stress. Examples of the magnetic field data which we have used in the two orbits presented here are given in Figure 2 and show the attitude problem very clearly. The upper panel shows the cross-track magnetic field data obtained on Day 164 of 1984. The sinusoidal modulation of the signal is due to one of the unfortunate attitude oscillation modes of the spacecraft. Another mode is clearly seen in the second panel using data obtained on Day 122 of the same year. Here a very long period attitude oscillation is seen in the signal. It is clear from these data, however, that signals of geophysical significance are present. On day 164, for example, the spacecraft passes through three large scale regions of field-aligned current as ascertained from the derivative of the magnetometer signal, ignoring the sinusoidal component. On day 122, three consecutive pairs of current sheets are visible, even in the presence of the long period perturbation.

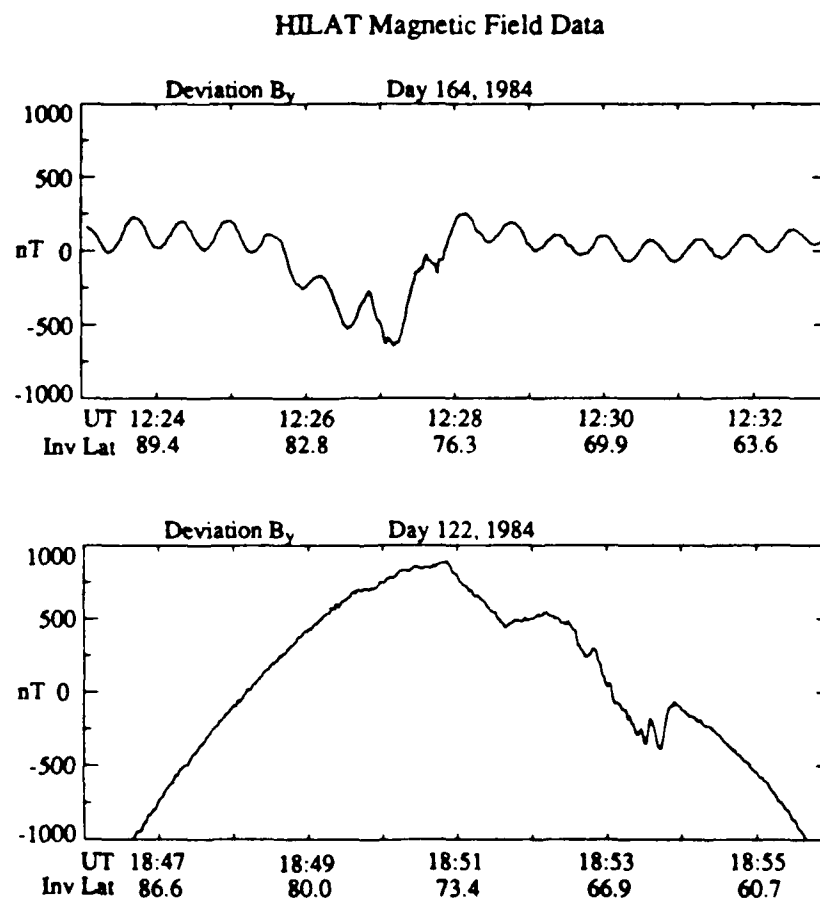


Figure 2. Magnetic field fluctuations measured by the HILAT satellite on days 164, and 122, 1984.

In the analysis below we have filtered the signals to remove these perturbing influences. A digital notch filter (order 20 Butterworth) with a center frequency of .0286 Hz and a bandwidth of .01 Hz was used for Day 164; a high pass filter allowing frequencies above 0.0029 Hz to contribute was used for both days. This necessary filtering precludes measurement of the largest scale size Poynting flux input to the high latitude system. The filtering scheme also results in errors at the end points of the time series and, therefore, we concentrate on the central portions of the plots below. The fractional orbit acquisitions from a real time satellite system such as HILAT are not suited for fully global measurements anyway; we are therefore restricted to more local studies such as auroral oval crossings. (For a case wherein the entire high latitude signatures of both E and B are available, the reader is referred to *Smiddy et al.*, 1977).

The Poynting flux measured on Day 164 is presented in the upper panel of Figure 3 along with a number of other measured parameters for this pass. The inset shows the pass in a magnetic local time invariant-latitude format. The satellite was acquired in the polar cap and passed over the dayside auroral oval just before local noon. Although MKS units were used in the derivation above, we have plotted the Poynting flux in $\text{ergs/cm}^2 \text{ sec}$ to conform to the usual notation in presenting particle fluxes in the aurora. The power flux is almost entirely downward throughout the pass, with the single exception of a brief burst of upward flux at $\sim 12:28 \text{ UT}$.

The second panel in Figure 3 is the field-aligned current derived from the magnetometer data using the usual assumptions for deriving the region1/region2 current patterns. Because a derivative is required some smoothing has been necessary. For the reasons mentioned above, we restrict attention to the three current sheets in the center of the figure and not the small variations outside this region which are most likely spurious. The existence of three sheets is quite common in the noon sector (*Iijima and Potemra*, 1978). The upward current sheet at invariant latitudes below about 72° is collocated with fairly hard electron precipitation as shown in the darkest trace in the third panel.

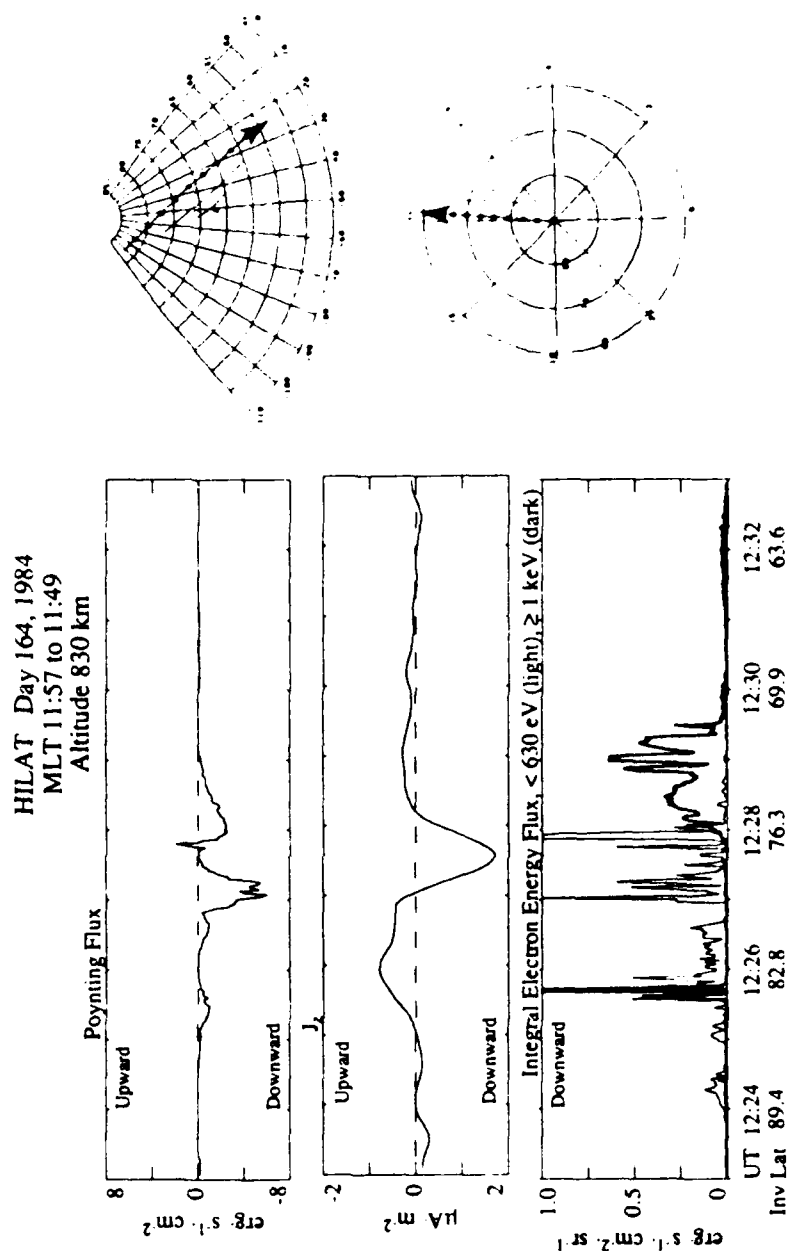


Figure 3. Poynting flux, field-aligned current, and precipitating electron energy flux measured on day 164. The panels on the right show the spacecraft trajectory in geographic (upper) and geomagnetic (lower) coordinates. The loci of the E- and F-region penetration of the ray path to the satellite are also indicated.

Except for three short time periods when the particle energy deposition briefly exceeded $1 \text{ erg/cm}^2 \text{ sec sr}$, the Poynting flux was at least 5 times the precipitating electron kinetic energy flux and usually was more than an order of magnitude larger. The particle influx has been plotted positive for downward energy flow since the detector pointed upward. Note that the plot of Poynting flux in the upper panel has the reverse polarity.

This orbit was such that the ionosphere was sunlit over the entire trajectory. From the solar depression angle, the solar-produced electron density and the conductivity of the E region can be determined. Although not particularly important in this case, we have also estimated and included the contribution of particle precipitation to the conductivity by assuming that the observed electron flux has been present long enough for a steady state electron density profile to be reached. With this estimate for Σ_p and the observed electric field from the ion drift meter we can estimate the Joule heating in the ionosphere and compare it to the Poynting flux as shown in Figure 4. We use the term "estimate" since the calculation cannot take into account the existence of any neutral wind in the region near 140 km where the Pedersen conductivity maximizes.

The comparison shows that the Poynting flux levels we have found are quite reasonable, and comparable to our estimate of the Joule heating rate. We argue here that the fundamental quantity of interest for studies of energy transfer to the atmosphere is the Poynting flux and that it can be remotely sampled on an orbital spacecraft.

Data from the second event is presented in Figure 5 in a format identical to that used in Figure 3. As can be seen in the raw data in Figure 2 and in the smoothed Birkeland currents in the second panel of Figure 5, several current sheets were detected during this dusk pass through the auroral oval. This is unusual, at least as far as the literature indicates. A significant upward current is collocated with a burst of electron precipitation. In this pass the ionosphere was not sunlit and hence its conductivity was determined primarily by the precipitation. Nonetheless, there was still significant Poynting flux in regions where the particle input was low and the Birkeland currents downward. The relative magnitudes of the kinetic energy and electromagnetic energy input are comparable in this case.

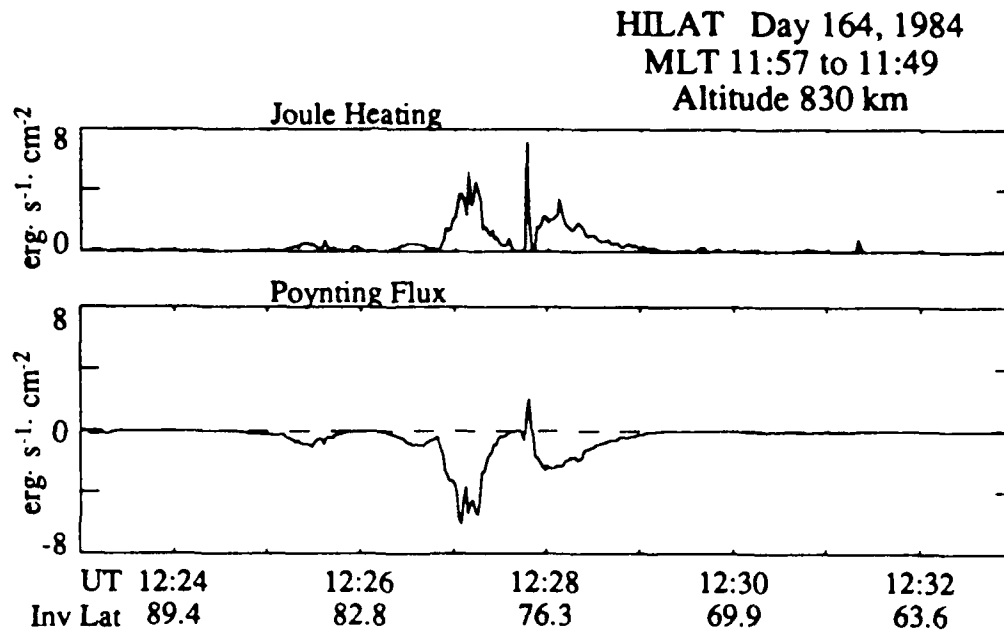


Figure 4. Comparison of the estimated Joule heating rate and Poynting flux measured by HILAT on day 164, 1984.

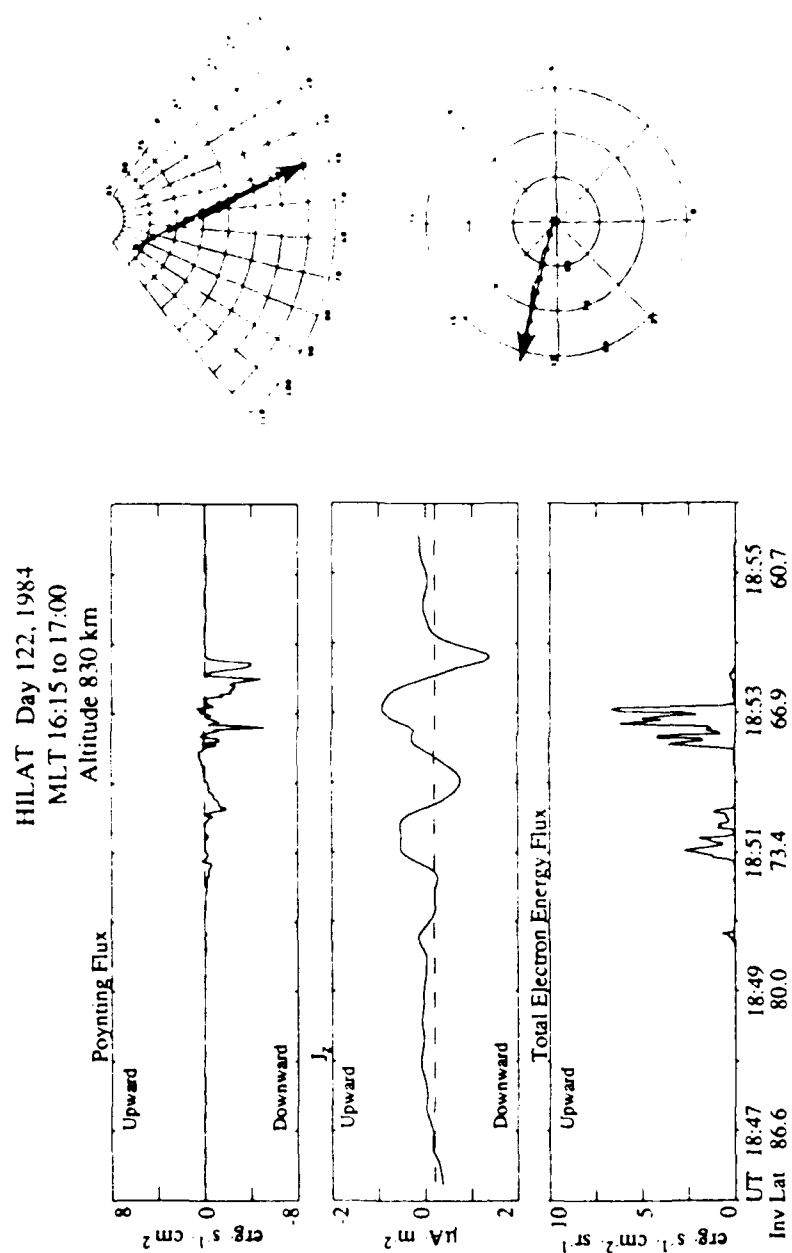


Figure 5. Poynting flux, field-aligned current, and precipitating electron energy flux measured on day 122, 1984.

It is essentially impossible to estimate the Joule heating in this case. In fact, an event such as this shows that even if the neutral wind is ignored or assumed to be unimportant, (a dubious contention), the electromagnetic energy input to the atmosphere cannot be ascertained simply from electric field and particle data. The Poynting flux yields the input unambiguously.

The two power sources are added together in Figure 6 to yield the total power input to the atmosphere via electrons and electromagnetic sources. It is unlikely that backscattered electrons or ions contribute very much to the energy balance and hence this plot represents the contribution of the solar wind magnetosphere interaction to the earth in this local time sector.

As was the case on Day 164, for a brief period of time there is evidence for upward Poynting flux at the edge of an electron precipitation zone.

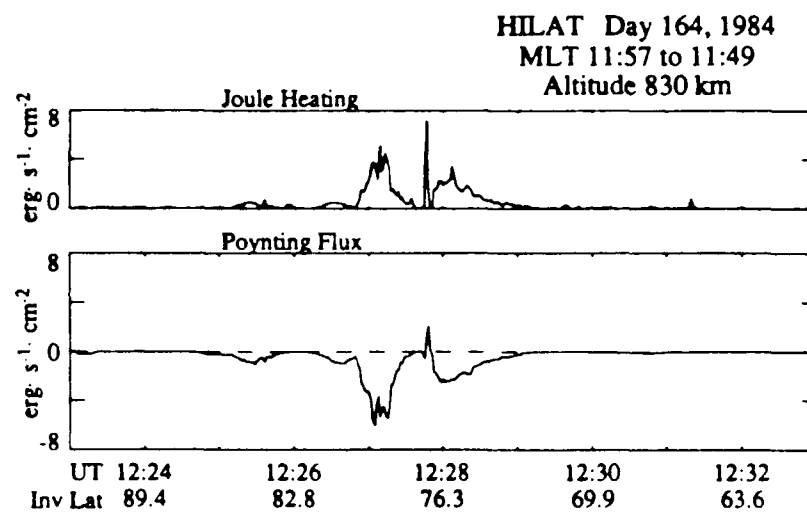


Figure 6. Sum of Poynting flux and total precipitating electron energy flux measured on day 122, 1984.

IV. AC POYNTING FLUX CONSIDERATIONS

As is pointed out in some detail in Appendix B, when one moves away from the quasi DC assumption and begins to consider temporally fluctuating electrodynamic quantities, the data become somewhat more difficult to interpret. In that appendix, we show that a spacecraft can be expected to measure a different electrodynamic signature for a steady-state field aligned current that closes in the ionosphere than it would for a purely propagating Alfvén wave. One can hope to separate these two special cases by examining the ratio of the measured electric- and magnetic-field fluctuations. For a steady-state current system closed in a uniform ionosphere, this ratio is proportional to the inverse of the ionospheric height-integrated Pedersen conductivity; For a pure Alfvén wave, this ratio yields the intrinsic impedance of the medium which in turn is directly related to the Alfvén speed. Fortunately, for the satellite orbits that we are considering, these characteristic numbers are significantly different – the inverse intrinsic impedance being ~ 0.1 mho, whereas the height-integrated ionospheric Pedersen conductivity is typically several mhos or more.

The top panels of Figures 7 and 8 show the power spectral density (PSD) of Poynting flux measured by the HILAT satellite between approximately 0.1 and 2 Hz for a small portion of two separate orbits. On the lower panels is the ratio $\mu_0 E/B$ measured over the same frequency range. The impedance implied from Figure 7 is close to the value corresponding to the inverse of the Pedersen conductance of the ionosphere. For Figure 8, the value is closer to the intrinsic impedance of the flux tube implied from the local plasma density and assuming the ion composition is 100% O^+ . These data are consistent with the signatures of steady state current systems closed in the ionosphere, and Alfvén waves, respectively.

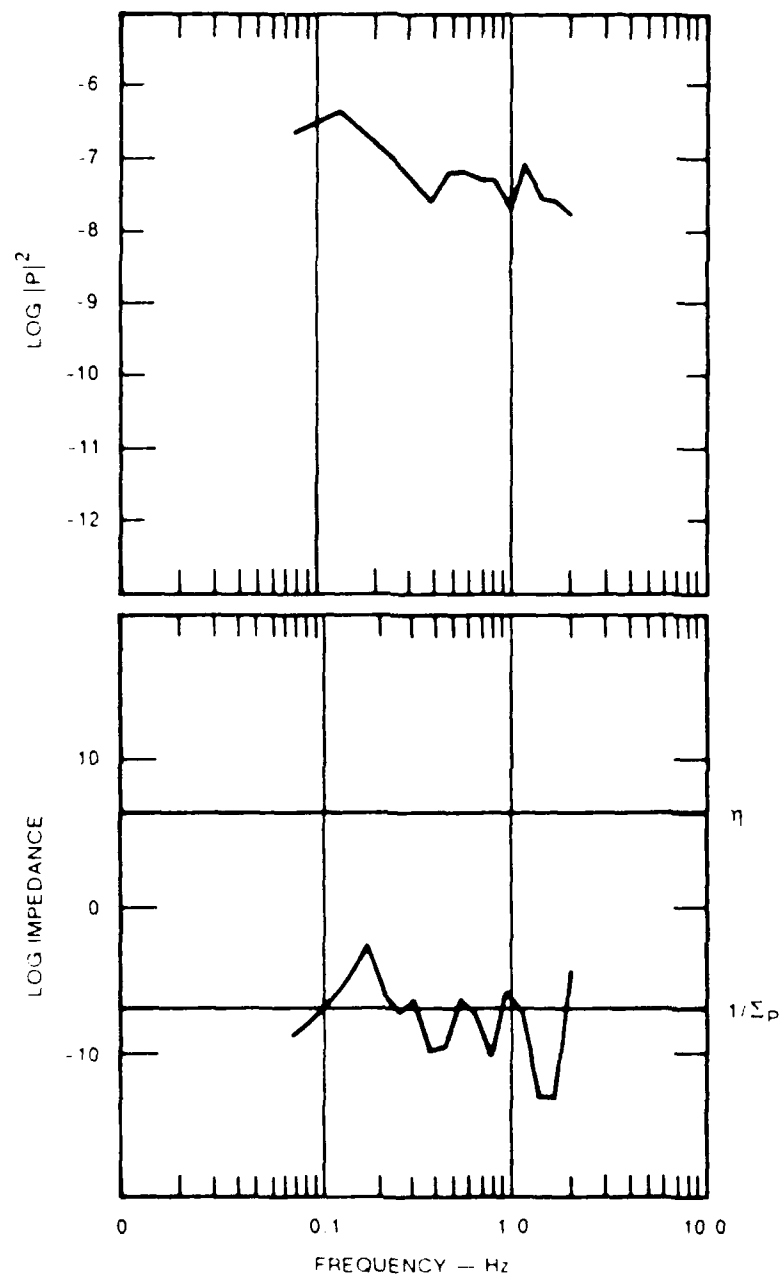


Figure 7. Power spectral density of Poynting flux and measured impedance for a steady state, ionospherically closed current system.

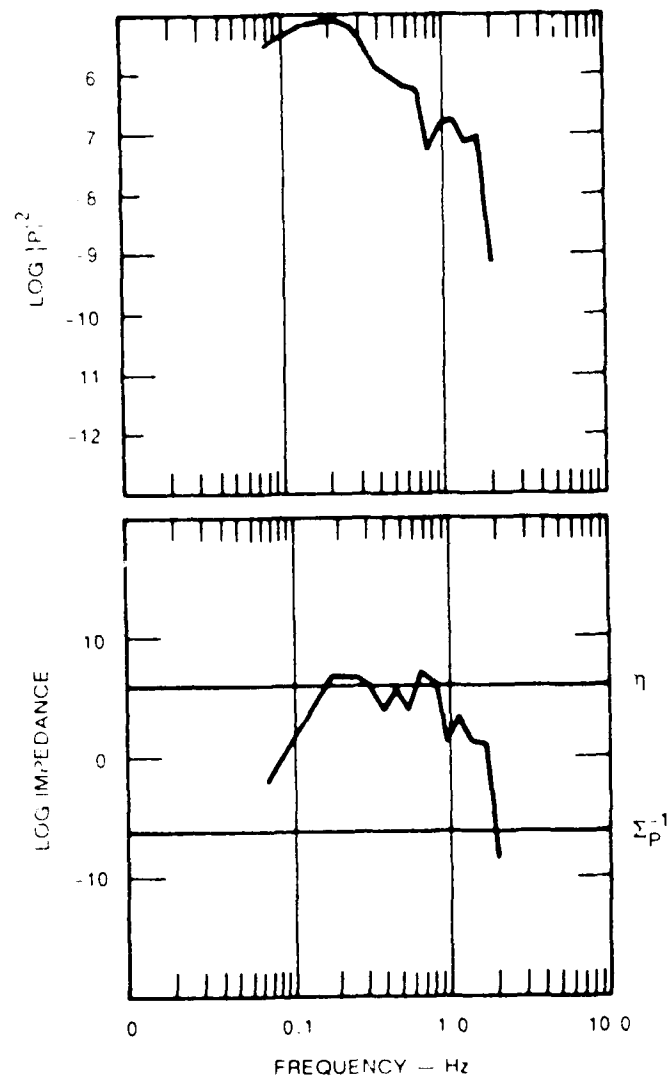


Figure 8. Power spectral density of Poynting flux and measured impedance for what appears to be an Alfvén wave.

However, many other orbits show values that are between these "limits" and even suggest that the impedance has a systematic frequency dependence. This implies a mixture of waves and ionospherically closed currents or, perhaps, interfering waves. At any rate a rich physical process is indicated, requiring much more detailed modelling than the simplistic derivation in Appendix B.

V. CONTINUED APPLICATIONS

We believe that the data and the theoretical discussion presented in this report show that a very important upper boundary condition dealing with energy input to the earth's atmosphere is measurable on a regular basis from orbiting spacecraft. If several satellites were available (e.g., DMSP) and instrumented to yield both the Poynting flux and the particle input, it seems feasible to obtain a near-continuous measure of the effect of the solar wind magnetosphere system on the earth's atmosphere. This in turn could be related to a number of parameters in upper atmospheric dynamics, the interplanetary magnetic field, sunspot number, the electric field in the lower atmosphere, and the like.

For the two cases studied here, we have shown that the electromagnetic power input to the upper atmosphere is larger than the kinetic energy input, much larger in the sunlit case. The calculated Poynting flux is consistent with estimates of the Joule heating in the case where we can estimate the latter. For both cases we have found significant energy input in regions with little electron precipitation.

Some localized regions displayed upward Poynting flux. This may be explained by something of a "flywheel" effect if the neutral atmosphere is put in motion by electrodynamic forcing and subsequently generates an electric field by a dynamo process. Such an effect is known to be responsible for electric fields in the low latitude ionosphere under quiet conditions, when solar heating drives the circulation in the upper atmosphere. In addition, a disturbance dynamo is also thought to occur when winds blow out of the auroral oval into the low latitude zone (*Fejer*, 1981). More detailed study of Poynting flux measurements may be an ideal method to ascertain whether this "flywheel" effect helps to maintain the circulation of the high latitude plasma, and over what time scale, when B_z turns southward.

VI. REFERENCES

1. Burke, W. J, M.S. Gussenhoven, M.C. Kelley, D.A. Hardy, and F.J. Rich, "Electric and Magnetic Field Characteristics and Discreet Arcs in the Polar Cap," *J. Geophys. Res.*, **87**, 1982.
2. Fejer, B. G., "The Equatorial Ionospheric Electric Fields: A Review," *J. Atmos. Terr. Phys.*, **43**, 1981.
3. Feynman, R.P., R.B. Leighton, and M. Sands, *The Feynman Lectures on Physics*, Addison-Wesley, 1964.
4. Iijima, T., and T. A. Potemra, "Large Scale Characteristics of Field-Aligned Currents Associated With Substorms," *J. Geophys. Res.*, **83**, 1978.
5. Mozer, F. S., and R. Serlin, "Magnetospheric Electric-Field Measurements with Balloons," *J. Geophys. Res.*, **74**, 1969.
6. Smiddy, M., M. C. Kelley, W. Burke, F. Rich, R. Sagalyn, B. Shuman, R. Hays, and S. Lai, "Intense Poleward Directed Electric Fields near the Ionospheric Projection of the Plasmapause," *Geophys. Res. Lett.*, **4**, 1977.
7. Sugiura, M., N.C. Maynard, W.H. Farthing, J.P. Heppner, B.G. Ledley, and L.J. Cahill, "Initial Results on the Correlation Between the Magnetic and Electric Fields Observed from the DE-2 Satellite in the Field-Aligned Current Regions," *Geophys. Res. Lett.*, **9**, 1982.
8. Vickrey, J.F., R.R. Vondrak, and S.J. Matthews, "Energy Deposition by Precipitating Particles and Joule Dissipation in the Auroral Ionosphere," *J. Geophys. Res.*, **87**, 1982

APPENDIX A.

DERIVATION OF THE POYNTING FLUX FOR A SIMPLE SITUATION

The concept of the Poynting flux as a diagnostic tool in the study of time-varying electromagnetic waves is well established. As discussed by Feynman et al. (1964), under certain circumstances the Poynting flux provides a valid conceptual measure of energy flow even for steady or DC electric and magnetic fields.

A formal derivation of Poynting's theorem begins with consideration of the total magnetic energy in some volume,

$$\epsilon_b = \left(\frac{1}{2\mu_o} \right) \int \int \int B^2 dV \quad (1)$$

The time rate of change of this quantity can be written

$$\frac{\partial \epsilon_b}{\partial t} = \frac{1}{\mu_o} \int \int \int \underline{B} \cdot \frac{\partial \underline{B}}{\partial t} dV \quad (2)$$

Using $\partial \underline{B} / \partial t = \underline{\nabla} \times \underline{E}$ and the vector identity $\underline{\nabla} \cdot (\underline{E} \times \underline{B}) = \underline{B} \cdot (\underline{\nabla} \times \underline{E}) - \underline{E} \cdot (\underline{\nabla} \times \underline{B})$ we have

$$\frac{\partial \epsilon_b}{\partial t} = -\frac{1}{\mu_o} \int \int \int \underline{\nabla} \cdot (\underline{E} \times \underline{B}) dV - \frac{1}{\mu_o} \int \int \int \underline{E} \cdot (\underline{\nabla} \times \underline{B}) dV \quad (3)$$

Finally, if we consider the static case $\partial \epsilon_b / \partial t = 0$ and furthermore, that $\underline{\nabla} \times \underline{B} = \mu_o \underline{J}$, we can write

$$\frac{1}{\mu_o} \int \int \int \underline{\nabla} \cdot (\underline{E} \times \underline{B}) dV = - \int \int \int (\underline{E} \cdot \underline{J}) dV \quad (4)$$

Finally, from Gauss' Theorem

$$\int \int \underline{P} \cdot d\hat{s} = \int \int \int (\underline{E} \cdot \underline{J}) dV \quad (5)$$

where $\underline{P} = 1/\mu_o(\underline{E} \times \underline{B})$ and the vector $d\hat{s}$ is pointed into the volume everywhere.

The classic example of this result is that of a long thin wire of resistance R carrying a current I across a voltage V . Since the magnetic field in this case is given by $B = \mu_o I / \pi a$ and $E = V/L$ where a is the wire radius and L is its length, the total energy flux into the wire is the surface integral of P ,

$$W = \int \int \underline{P} \cdot d\hat{s} = \frac{1}{\mu_o} \left(\frac{V}{L} \right) \left(\frac{\mu_o I}{2\pi a} \right) (2\pi L) = VI \quad (6)$$

which yields the total energy dissipated per unit time in the volume. Obviously, in deriving this result we have ignored the fringing fields and the contributions at the ends of the thin wire.

APPENDIX B

Derivation of the Expected Characteristics of Electric- and Magnetic-Field Fluctuation Signatures for Steady State Currents and Alfvén Waves

Combined measurements of \bar{E} , \bar{B} , local N_e and Σ_P can distinguish between steady state currents and Alfvén waves.

Let's examine what a spacecraft observes for these two cases.

When one considers a quasi-DC situation, it is clear that a steady state is assumed.

However, when temporal variations are included:

Assume: $J = J_{ss} + J_{TV}$; $J_{TV} \propto e^{i\omega_o t}$

Where J_{ss} = steady state, J_{TV} = temporally varying

$$\begin{aligned}\nabla \times \bar{B} &= \mu_o (J_{ss} + J_{TV}) \\ &= \nu_o \left(J_{ss} + \epsilon \frac{\partial \bar{E}}{\partial t} \right)\end{aligned}\tag{1}$$

$$\epsilon = \frac{NM}{|B|^2} \Rightarrow V_A = \frac{1}{\sqrt{\mu_o \epsilon}}$$

Vector Identity

$$\nabla \times \nabla \times \bar{B} = \nabla (\nabla \cdot \bar{B}) - \nabla^2 \bar{B} \quad (2)$$

$$\nabla \times \bar{E} = -\frac{\partial \bar{B}}{\partial t} \quad (3)$$

Combine (1), (2), and (3):

$$\nabla^2 \bar{B} - \mu_o \epsilon \frac{\partial^2 \bar{B}}{\partial t^2} = -\mu_o \nabla \times J_{ss} \quad (4)$$

Equation (4) is true for waves or steady-state. Solving (4) for steady state conditions

$$J_{ss} = \frac{ik_{ssx}}{\mu_o} B_{ys} \quad (5)$$

Steady State \Rightarrow The current must close in the ionosphere.

$$\nabla \cdot J \equiv 0 \quad ; \quad \text{Assume } \frac{\partial}{\partial y} \rightarrow 0$$

$$J_{ss} = \nabla_{\perp} \cdot (\Sigma_P \bar{E}) = \frac{\partial}{\partial x} (\Sigma_P E_z)$$

$$\text{Assume } \Sigma_P \propto e^{ik^{\Sigma xs} x} \quad ; \quad E_z \propto e^{ik_{xss} x}$$

$$\Rightarrow J_{ss} = (i k^{\Sigma xs} + i k_{xss}) \Sigma_P E_z = \frac{ik_{xss}}{\mu_o} B_{ys}$$

$$\left| \frac{E_z}{B_y} \right| = \frac{1}{\mu_o} \left(\frac{k_{ssx} + k^{\Sigma_{sx}}}{k_{ssx}} \right) \frac{1}{\Sigma_P} \quad (6)$$

In summer $k^{\Sigma_{sx}} \Rightarrow 0 \Rightarrow \left| \frac{E_z}{B_y} \right| = \frac{1}{\mu_o \Sigma_P}$

Steady State Variations: $\frac{E_z}{B_y} \Rightarrow$ IONOSPHERIC IMPEDANCE!

Pure Alfvén Wave Signature

$$\bar{E}, \bar{B} \propto e^{i(\omega_A t - k_{xA}x - k_{zA} \cdot z)}$$

$$\nabla \times \bar{E} = -\frac{\partial \bar{B}}{\partial t}$$

Assume $E_z = 0$, $\frac{\partial}{\partial y} \Rightarrow 0$

$$\nabla \times \bar{E} = \hat{x} \left(\frac{\partial E_z}{\partial y} - \frac{\partial E_y}{\partial z} \right) - \hat{y} \left(\frac{\partial E_z}{\partial x} - \frac{\partial E_x}{\partial t} \right) + \hat{z} \left(\frac{\partial E_y}{\partial x} - \frac{\partial E_x}{\partial y} \right)$$

$$\hat{x} : ik_{zA} E_y = \omega_A B_z$$

$$\hat{y} : ik_{xA} E_x = \omega_A B_y \Leftarrow E_x, B_y$$

Measurable by a spacecraft!

$$\hat{z} : ik_{xA} E_y = \omega_A B_z$$

$$\left| \frac{E_x}{B_y} \right| = \frac{\omega_A}{k_{zA}} = V_A = \frac{1}{\sqrt{\mu\epsilon}}$$

$$\left| \frac{E_x}{B_y} \right| = \frac{\eta}{\mu_o} ; \quad \eta = \text{INTRINSIC IMPEDANCE OF THE MEDIUM!}$$

A spacecraft measures only with respect to x and hence, only one component of (4)

$$\nabla^2 B_y - \frac{1}{V_A^2} \frac{\partial^2 B_y}{\partial t^2} = \mu_o \frac{\partial J_{ss}}{\partial x} \quad (4')$$

Steady-State Spatial Variations

$$B_y \propto e^{i(\omega t - k_{zss} \cdot x)}$$

plug into (4')

$$(-ik_{zss})^2 B_{ys} = -i\mu_o k_{zss} J_{ss}$$

$$B_{ys} = \frac{-i\mu_o J_{ss}}{k_{zss}} \quad (5)$$

For an O^+ plasma at 800 km altitude

$$\eta \simeq \frac{3.8 \times 10^5}{(N_e)^{\frac{1}{2}}}$$

N_e	η (ohms)	$\frac{1}{\eta}$ (mhos)
10^3	12.0	.08
10^4	3.8	.26
10^5	1.2	0.8

$$\Sigma_P \sim 1 - 10 \text{ mhos!}$$